

Assembly of a Nanogold-Assisted Aptamer Sensor for Highly Sensitive Detection of Homocysteine

Shaoshuai Wang¹, Yingzi Mi², Guoyong Ren², Yanjun Chen², Xuemei Wu^{2,*}

¹ Department of Neurology, The First Hospital of Shanxi Medical University, Taiyuan, Shanxi 030012, China.

² Department of Neurology, General Hospital of Tisco, Taiyuan, Shanxi 030008, China.

*E-mail: xuemeiwu0621@163.com

Received: 12 August 2021 / Accepted: 4 September 2021 / Published: 10 October 2021

With more in-depth exploration on stroke risk factors in recent years, an increasing number of studies show that homocysteine (HCY) is a new risk factor of cerebral infarction. In this work, graphene was adopted for the modification of glassy carbon electrodes, and gold nanoparticles were modified onto the graphene surface with a simple and controlled electrodeposition method, followed by aptamer immobilization, to construct the homocysteine electrochemical sensor. Under optimum conditions, the analytical performance of the proposed aptamer sensor showed a positive response to different concentrations of HCY. The peak currents were proportional to HCY concentration. The linear regression equation can be found from 0.05–20.0 μM . The limit of detection can be calculated to be 5 nM based on $S/N=3$.

Keywords: Homocysteine; Aptamer; AuNPs; Graphene; Cerebral infarction

1. INTRODUCTION

Due to the characteristics of high incidence, high morbidity, high recurrence rate and high mortality, cerebral infarction has become a severe disease which is significantly harmful to human health [1–4]. Traditional risk factors that are associated with the occurrence of cerebral infarction include hypertension, diabetes mellitus, smoking, alcohol addiction, obesity and dyslipidemia [5–7]. However, an increasing number of studies in recent years show that homocysteine (HCY) is a new risk factor of ischemic stroke, which is of great importance [7–10].

HCY is a low molecular weight amino thiol in living organisms and is an essential amino acid. It is not available through food intake, but is an intermediate product from the metabolism of methionine. In living organisms, HCY is cross-linked to cysteine, reduced glutathione, and proteins in the form of disulfide bonds [11–14]. The total concentration of homocysteine in a biological sample refers to the

sum of the concentrations of all the above-mentioned types of homocysteine. The normal value of total homocysteine concentration in human plasma usually ranges from 5.0 to 16.0 $\mu\text{mol/L}$. Therefore, a rapid, highly sensitive and accurate determination of HCY can provide important supporting information for the diagnosis of clinically relevant diseases [11,15–20]. Previously reported methods for the determination of homocysteine include high performance liquid chromatography (HPLC), capillary electrophoresis (CE), gas chromatography (GC), fluorescence spectrometry, immunoassay, molecularly imprinted fluorescence sensing, and electrochemical sensing [21–23], among which electrochemical sensing methods have received more attention for their simplicity of operation, low cost, high sensitivity, rapid response, and ease of miniaturization and automation [24,25].

Electrochemical aptamer sensors are based on the specific binding of aptamer to the target, using the nucleic acid aptamer as a recognition element or detection object, and converting the signal generated in the aptamer molecule-specific recognition into an electrical signal through the action of a transducer. The nucleic acid aptamer is first immobilized on the surface of a functionally activated electrode by adsorption, covalent bonding, and self-assembly [26,27]. The immobilization effect of the aptamer is directly related to the choice of the functionalization strategy of the electrode surface, and the effect of the site-resistance phenomenon should be minimized. The aptamer bound to the target changes the electrode surface structure. The electrochemical signal changes, according to which the quantitative detection of the target is performed. Based on detection methods, electrochemical aptamer biosensors can also be classified as conductive, current, capacitive, potentiometric, and impedance types [28–30], which are fast, sensitive, specific, simple, portable, cost-effective, and miniaturized, making them a promising analytical tool [31,32].

Graphene is a typical two-dimensional carbon nanomaterial with a unique sp^2 hybridized crystal structure and honeycomb structure. With the large number of ions possessed by the presence of ionic π -bonds in the molecule, graphene has extraordinary electronic and electrical properties. It has been reported to be applied in electrochemical and biosensing detection of biomolecules such as NO, glucose, DNA, ascorbic acid, dopamine, proteins, and L-cysteine [33,34]. Due to their unique chemical, electronic and optical properties and good biocompatibility, gold nanoparticles are widely used in biomedical sensing, tumor therapy, biomarkers, heavy metal analysis, chemical catalysis and other fields [35,36]. In this work, an HCY aptamer electrochemical sensor was constructed based on a gold nanoparticle-graphene composite membrane. On the one hand, with the large specific surface area of gold nanoparticles and graphene being nanomaterials, the effective area of the modified electrode and the enrichment of HCY on the surface of the chemically modified electrode can be increased to improve the detection sensitivity of the sensor; on the other hand, the good electrical conductivity of gold nanoparticles and graphene can promote the electron transfer rate between HCY and the surface of the chemically modified electrode, thus shortening the response time of the sensor.

2. EXPERIMENTAL

2.1. Reagents and Instruments

The oligonucleotides were purchased from Hongxun Technology Co. The sequence is as follows:

5'SH-(CH₂)₆ ACCA GCAC ATTC GATT ATAC CAGC TTAT TCAA TTCA CAGC TATG TCCT ATAC CAGC TTAT TCAATT-3'.

Graphene oxide dispersion was purchased from Xianfeng Nano Co. with a concentration of 1 mg/mL. HCY was purchased from Tricia (Shanghai) Chemical Industry Development Co. H₂AuCl₄·4H₂O was purchased from Shanghai Chemical Reagent Co. All the other chemicals were analytical grade and can be used without purification.

Preparation of 0.25 M phosphate buffer solution (PBS): 50g NaCl, 1.25g KCl, 22.375g Na₂HPO₄·12H₂O, and 1.5g KH₂PO₄ were dissolved in 200 mL of ultrapure water, the solution pH of the solution was adjusted to 7.0, and the volume was fixed to 250 mL.

All the electrochemical experiments were conducted in the CHI660D electrochemical workstation (Shanghai Chenhua Instruments Co., Ltd.). A PHS-3E meter (Shanghai Youke Instrument Co., Ltd.) is used for pH detection. Scanning electron microscopy (SEM) was performed on a FEI-Sirion 200 field emission scanning electron microscope.

2.2. Preparation of aptamer electrochemical sensor

First of all, the glassy carbon electrode (GCE) was polished with alumina powder, sonicated in nitric acid and acetone with a proportion of 1:1, and washed with double distilled water. 3 μL of graphene dispersion was applied dropwise to the GCE surface and dried at room temperature. The dried electrode was inserted into PBS with cyclic voltammetric scanning for 20 turns at 0--1.5 V, allowing the reduction of graphene oxide (denoted as G/GCE). AuNPs were modified by electrochemical deposition, in which G/GCE was immersed in 5 mM H₂AuCl₄ and 0.1 M KNO₃ with a potential of 400 mV applied over 200 s (denoted as Au/G/GCE). 5 μL of 2 μM aptamer solution was applied dropwise to the Au/G/GCE surface to complete the self-assembly of thiol inducers. The modified glassy carbon electrode was immersed in 1 mM 6-mercapto-1-hexanol solution for 1 h and rinsed with 0.1 M PBS solution at pH 7.4 to limit the non-specific binding sites (denoted as aptamer/G/GCE).

2.3. HCY sensing

A three-electrode system was adopted for all tests. The saturated mercury electrode (SCE) was used as the reference electrode and the platinum electrode was used as the counter electrode. The detection substrate was 0.25 mol/L PBS (pH = 7.0), the scanning potential range was -0.2 V to 0.8 V, the enrichment potential was -0.2 V, and the enrichment time was 40 s. Lyophilized serum was reconstituted with 5.0 ml Milli-Q water. After complete dissolution, a 500 μL aliquot was treated with 500 μL 10% (w/v) sodium borohydride solution by incubation at 50 °C within 30 min. Afterwards, 1250 μL HClO₄-water solution with a proportion of 1:4 was added and the mixture was homogenized by stirring and centrifuged at 3000 rpm for 10 min. In the next step, the liquid was filtered through a Nylon membrane. The determination of HCY was then carried out with electrochemical method.

3. RESULTS AND DISCUSSION

To investigate the electrocatalytic mechanism of gold nanoparticles modified graphene carbon paste electrode for homocysteine, the surface morphology of different electrodes was characterized with the scanning electron microscopy technique, and the results are shown in Figure 1A, in which the surface of G/GCE is flat (Figure 1A). After electrodeposition of gold nanoparticles, the electrode surface became sparser and a large number of gold nanoparticles could be observed (Figure 1B). A number of important studies also show that the combination of graphene with other metal nanoparticles (NPs) offers opportunities for developing graphene-based hybrids as enhanced materials to construct a new type of high-performance electrochemical sensing platform [37,38]. Both the sparse structure of the electrode surface and the nano-effect of graphene and gold nanoparticles are beneficial to the increase of the specific surface area of the electrode and the improvement of the effective enrichment of HCY by the sensor. In addition, gold has a good affinity with the sulfhydryl group being in the HCY structure, which can effectively ensure the specificity of the sensor for HCY detection.

To further confirm the successful electrodeposition of gold nanoparticles, an energy dispersive X-ray (EDX) spectroscopic characterization of different electrodes was performed in this study. The elements presenting on the surface of G/GCE include C, O, Cl and K, among which C element is mainly derived from graphene, O element is mainly derived from graphene oxide, the content of Cl and K elements is quite low and they should be impurity elements in graphene oxide. Correspondingly, the elements presenting on the surface of gold nanoparticle-modified graphene carbon paste electrode are C, O, Au, Cl and K, among which the main sources of C and O are the same as those on G/GCE, while Cl and K are not only from the impurities of graphene oxide, but also from AuCl_4^- and supporting electrolyte solutions left on the electrode surface. Au elements may originate from nanogold or AuCl_4^- residues on the electrode surface, but the Au content on the electrode surface is high. Based on the content of Cl on the electrode surface, it can be inferred that the content of Au from AuCl_4^- is very low, which indicates that the Au element on the electrode surface is mainly derived from nano-gold, and also suggests that nano-gold is successfully modified to the electrode surface.

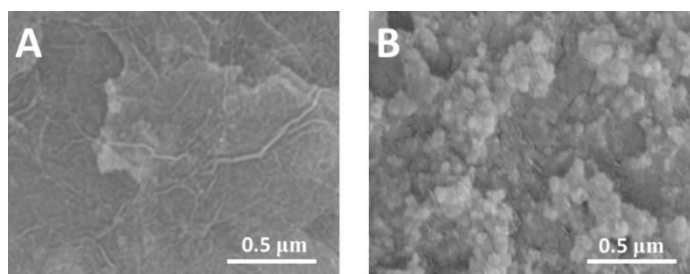


Figure 1. SEM image of (A) G/GCE and (B) Au/G/GCE.

The electrochemical properties of different electrodes were investigated using $\text{K}_3[\text{Fe}(\text{CN})_6]/\text{K}_4[\text{Fe}(\text{CN})_6]$ as molecular probes, and the results are shown in Figure 2. On G/GCE, a pair

of redox peaks with good peak shape was observed, where the peak potential of the oxidation peak was $E_{pa} = 0.30$ V and the peak current was $I_{pa} = 1.4$ μ A, while the peak potential of the reduction peak was $E_{pc} = 0.20$ V and the peak current was $I_{pc} = 1.5$ μ A. On Au/G/GCE, a pair of redox peaks with good peak shape was also observed. It is clear that the modification of gold nanoparticles significantly improved the electrochemical response of the molecular probe, the possible reason of which is that the modification of gold nanoparticles changed the surface structure of the electrode and effectively increased the specific surface area of the electrode [39,40], being consistent with the results of SEM characterization.

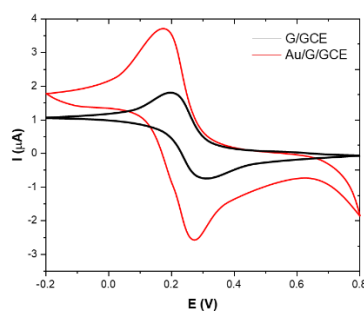


Figure 2. CVs of bare G/GCE and Au/G/GCE in 5 mM $K_3[Fe(CN)_6]/K_4[Fe(CN)_6]$ and 1 M KCl solution.

In order to make the aptamer sensor be sensitive enough, many parameters need to be optimized and the concentration of the aptamer was first optimized. As shown in Figure 3, an additional 0.1 μ M of HCY in the range of 0.5 to 5 μ L was detected. The current values of the assay show an increase with the concentration, peaking at 4 μ L. Subsequently, the current intensity decreases with the increase of aptamers. Therefore, we chose 4 μ L as the optimal concentration.

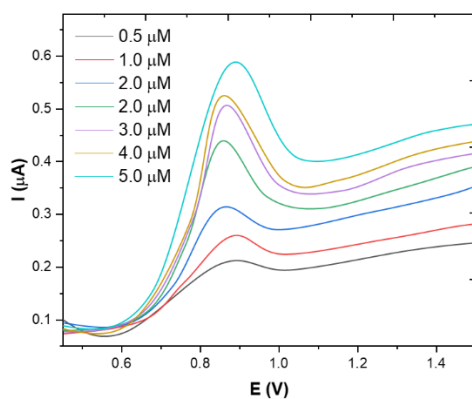


Figure 3. DPV curves of aptamer/G/GCE in solution with different concentrations of aptamer in 0.1 M PBS (pH = 7.0).

The type of buffer solution was also optimized. Citrate, acetate and phosphate buffer solutions were adopted for the detection of HCY at 0.1 μM . As shown in Figure 4, the aptamer sensor has the highest current value in 0.1 M PBS, which is in agreement with previous reports [41,42]. Therefore, PBS was selected as the supporting electrolyte.

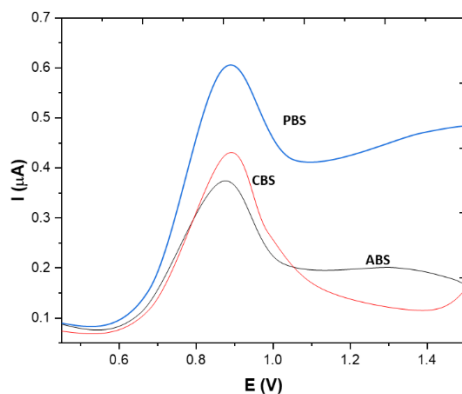


Figure 4. DPV curves of aptamer/G/GCE towards 0.1 μM HCY in PBS, ABS and CBS.

The effect of the concentration of PBS was also investigated in this study. As shown in Figure 5, the concentration of PBS does not particularly affect the detection signal, although the highest current values were measured in 0.25M. Therefore, 0.25 M PBS was chosen as the electrolyte.

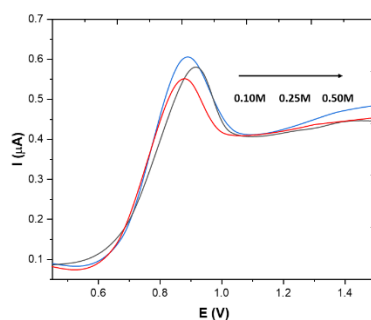


Figure 5. DPV curves of aptamer/G/GCE towards 0.1 μM HCY with different concentrations of PBS.

Under optimum conditions, the analytical performance of the aptamer/G/GCE was tested. As shown in Figure 6, the aptamer/G/GCE had a positive response to different concentrations of HCY. The peak currents were proportional to HCY concentration. The linear regression equation can be found from 0.05–20.0 μM . The limit of detection can be calculated to be 5 nM based on $S/N=3$. Table 1 shows the sensing performance of our proposed aptamer sensor with previous reports, which indicates that the aptamer/G/GCE has demonstrated a highly competitive performance.

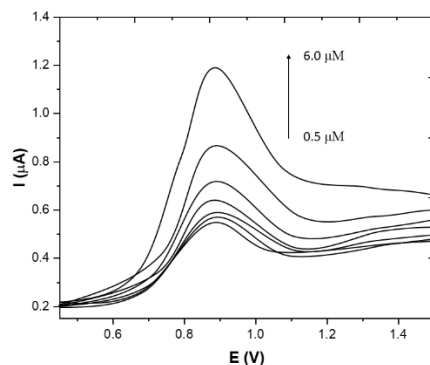


Figure 6. DPV curves of aptamer/G/GCE towards 0.5, 1.0, 2.0, 3.0, 4.0, 5.0, and 6.0 μM HCY.

Table 1. Comparison of aptamer/G/GCE with other electrochemical sensors toward HCY sensing

Sensor	Linear range	Limit of detection	Reference
Aucoll-Cyst-CPE	20-120 nM	-	[43]
Carbon nanotube/GCE	1-60 μM	60 nM	[44]
Carbon-nanotube paste	5-200 μM	4.6 μM	[45]
Au NPs/graphene sponge	1-100 μM	-	[46]
AuNP/rGO/GCE	2-14 mM	6.9 μM	[47]
RGO-TiO ₂ -based GCE	1-80 μM	24 nM	[48]
aptamer/G/GCE	0.05-20.0 μM	5 nM	This work

The interference immunity of the sensor was also evaluated. The results showed that 10-fold Cl^- , 5-fold Na^+ , K^+ , Ca^{2+} , 1.3-fold Mg^{2+} , 0.1-fold ascorbic acid and uric acid did not interfere with the determination of 100 μM HCY (the signal variation was less than $\pm 5\%$), which indicates that the sensor has good anti-interference ability for inorganic ions, however, the anti-interference ability for biological small molecules should be further improved.

In addition, the stability and reproducibility of the aptamer sensor were investigated. When the sensors were placed for 7 d and measured in parallel, the detection signal could still be maintained at 93.5% of the initial signal, indicating that the aptamer sensors have good stability. Meanwhile, the relative standard deviation was 4.4%, indicating that the sensor has good reproducibility.

The developed aptamer/G/GCE was applied to the determination of HCY in a serum sample and the sample treatment procedure was conducted on the basis of the reduction of disulfides and release of the protein-bound homocysteine. In order to evaluate the accuracy of the method, 5 μM of each samples spiked with a known concentration were prepared. Recovery studies yielded a mean concentration ($n = 5$) for HCY in the serum sample after spiking, of $5.2 \pm 0.2 \mu\text{M}$, which means a recovery rate of $104 \pm 4\%$.

4. CONCLUSION

In this work, graphene was adopted for the modification of glassy carbon electrodes and gold nanoparticles were modified onto the graphene surface with a simple and controlled electrodeposition

method, followed by aptamer immobilization, to construct the HCY electrochemical sensing interface. The electrochemical technology characterization showed that the gold nanoparticle-graphene composite film had a significant catalytic effect on the electrochemical reaction of HCY. The nanocomposite membranes were characterized by scanning electron microscopy and energy dispersive X-ray spectroscopy. In addition, the reaction mechanism of HCY at the sensing interface was investigated, and the performance of the sensor was evaluated. The results reveal that the basic performance of the sensor is good, however, the anti-interference ability of the sensor against small biological molecules needs to be further improved, which limits its application in biomedical field to some extent.

ACKNOWLEDGEMENTS

This work was supported by Metallurgical Safety and Health Branch of China Metal Society Health and Health Research Projects(Fund number:jkws201848).

References

1. J. Anniwaer, M. Liu, K. Xue, A. Maimaiti, A. Xiamixiding, *Int. J. Neurosci.*, 129 (2019) 654.
2. R. Duan, X. Fang, D. Wang, *Front. Chem.*, 9 (2021) 361.
3. C. Li, F. Sun, *Front. Chem.*, 9 (2021) 409.
4. J. Li, S. Zhang, L. Zhang, Y. Zhang, H. Zhang, C. Zhang, X. Xuan, M. Wang, J. Zhang, Y. Yuan, *Front. Chem.*, 9 (2021) 339.
5. Y. Cao, N. Su, D. Zhang, L. Zhou, M. Yao, S. Zhang, L. Cui, Y. Zhu, J. Ni, *Eur. J. Neurol.*, 28 (2021) 1931.
6. W. Li, W. Luo, M. Li, L. Chen, L. Chen, H. Guan, M. Yu, *Front. Chem.*, 9 (2021) 610.
7. J. Liu, T. Yang, J. Xu, Y. Sun, *Front. Chem.*, 9 (2021) 488.
8. H. Fan, S. Yang, Y. Li, J. Yin, W. Qin, L. Yang, J. Yuan, W. Hu, *Eur. Neurol.*, 79 (2018) 54.
9. L. Gungor, M. Polat, M.B. Ozberk, B. Avci, U. Abur, *J. Stroke Cerebrovasc. Dis.*, 27 (2018) 1921.
10. Y. Wang, L. Chen, T. Xuan, J. Wang, X. Wang, *Front. Chem.*, 9 (2021) 569.
11. Z. Wu, J. Liu, M. Liang, H. Zheng, C. Zhu, Y. Wang, *Front. Chem.*, 9 (2021) 208.
12. B. Fan, Q. Wang, W. Wu, Q. Zhou, D. Li, Z. Xu, L. Fu, J. Zhu, H. Karimi-Maleh, C.-T. Lin, *Biosensors*, 11 (2021) 155.
13. L. Fu, Z. Liu, J. Ge, M. Guo, H. Zhang, F. Chen, W. Su, A. Yu, *J. Electroanal. Chem.*, 841 (2019) 142.
14. L. Fu, W. Su, F. Chen, S. Zhao, H. Zhang, H. Karimi-Maleh, A. Yu, J. Yu, C.-T. Lin, *Bioelectrochemistry* (2021) 107829.
15. S. Yan, Y. Yue, L. Zeng, L. Su, M. Hao, W. Zhang, X. Wang, *Front. Chem.*, 9 (2021) 220.
16. L. Fu, Q. Wang, M. Zhang, Y. Zheng, M. Wu, Z. Lan, J. Pu, H. Zhang, F. Chen, W. Su, *Front. Chem.*, 8 (2020) 92.
17. L. Fu, A. Wang, K. Xie, J. Zhu, F. Chen, H. Wang, H. Zhang, W. Su, Z. Wang, C. Zhou, S. Ruan, *Sens. Actuators B Chem.*, 304 (2020) 127390.
18. W. Wu, Q. Zhou, Y. Zheng, L. Fu, J. Zhu, H. Karimi-Maleh, *Int J Electrochem Sci*, 15 (2020) 10093.
19. W. Wu, M. Wu, J. Zhou, Y. Xu, Z. Li, Y. Yao, L. Fu, *Sens. Mater.*, 32 (2020) 2941.
20. Y. Xu, Y. Lu, P. Zhang, Y. Wang, Y. Zheng, L. Fu, H. Zhang, C.-T. Lin, A. Yu, *Bioelectrochemistry*, 133 (2020) 107455.
21. J. Zhou, Y. Zheng, J. Zhang, H. Karimi-Maleh, Y. Xu, Q. Zhou, L. Fu, W. Wu, *Anal. Lett.*, 53 (2020) 2517.

22. H. Beitollahi, S.Z. Mohammadi, M. Safaei, S. Tajik, *Anal. Methods*, 12 (2020) 1547.
23. V.R.R. Bernardo-Boongaling, N. Serrano, J.J. García-Guzmán, J.M. Palacios-Santander, J.M. Díaz-Cruz, *J. Electroanal. Chem.*, 847 (2019) 113184.
24. K.S. Devi, M. Sasya, U.M. Krishnan, *TrAC Trends Anal. Chem.*, 125 (2020) 115838.
25. T.Y. Hung, J. Lin, *IEEE Sens. Lett.*, 1 (2017) 1.
26. X. Pang, H. Bai, D. Xu, J. Ding, W. Fan, W. Shi, *Appl. Surf. Sci.*, 564 (2021) 150397.
27. G. Ziyatdinova, E. Kozlova, H. Budnikov, *Electrochimica Acta*, 270 (2018) 369.
28. H.J. Kim, K.-S. Lee, Y.-J. Jeon, I.-S. Shin, J.-I. Hong, *Biosens. Bioelectron.*, 91 (2017) 497.
29. H. Kivrak, K. Selçuk, O.F. Er, N. Aktas, *Mater. Chem. Phys.*, 267 (2021) 124689.
30. A. Nosal-Wiercińska, M. Wiśniewska, M. Grochowski, W. Kaliszczak, S. Skrzypek, M. Brycht, D. Guziejewski, W. Franus, *Adsorpt. Sci. Technol.*, 35 (2017) 396.
31. R. Rajaram, P. Kanagavalli, S. Senthilkumar, J. Mathiyarasu, *Biotechnol. Bioprocess Eng.*, 25 (2020) 715.
32. S.-Y. Yu, Y. Gao, F.-Z. Chen, G.-C. Fan, D.-M. Han, C. Wang, W.-W. Zhao, *Sens. Actuators B Chem.*, 290 (2019) 312.
33. H. Beitollahi, S.Z. Mohammadi, M. Safaei, S. Tajik, *Anal. Methods*, 12 (2020) 1547.
34. L. Hosseinzadeh, A. Khoshroo, K. Adib, M. Rahimi-Nasrabadi, F. Ahmadi, *Microchem. J.*, 165 (2021) 106124.
35. N. Nioradze, T. Dolidze, M. Shushanian, D. Khoshtariya, *J. Electroanal. Chem.*, 855 (2019) 113490.
36. M. Thangamuthu, W.E. Gabriel, C. Santschi, O.J. Martin, *Sensors*, 18 (2018) 800.
37. X. Zhou, J. Zhang, Z. Pan, D. Li, *Crit. Rev. Anal. Chem.*, 49 (2019) 1.
38. Y. Yuan, Y. Wang, H. Wang, S. Hou, *J. Electroanal. Chem.*, 855 (2019) 113495.
39. M. Pourmadadi, J.S. Shayeh, M. Omid, F. Yazdian, M. Alebouyeh, L. Tayebi, *Microchim. Acta*, 186 (2019) 1.
40. J. Ying, Y. Zheng, H. Zhang, L. Fu, *Rev. Mex. Ing. Quím.*, 19 (2020) 585.
41. H.-M. Zhang, X.-L. Zhou, R.-T. Hui, N.-Q. Li, D.-P. Liu, *Talanta*, 56 (2002) 1081.
42. S. Melnyk, M. Pogribna, I.P. Pogribny, P. Yi, S.J. James, *Clin. Chem.*, 46 (2000) 265.
43. L. Agüí, C. Peña-Farfal, P. Yáñez-Sedeño, J.M. Pingarrón, *Talanta*, 74 (2007) 412.
44. K. Gong, Y. Dong, S. Xiong, Y. Chen, L. Mao, *Biosens. Bioelectron.*, 20 (2004) 253.
45. N.S. Lawrence, R.P. Deo, J. Wang, *Talanta*, 63 (2004) 443.
46. X.-H. Wen, X.-F. Zhao, B.-F. Peng, K.-P. Yuan, X.-X. Li, L.-Y. Zhu, H.-L. Lu, *Appl. Surf. Sci.*, 556 (2021) 149735.
47. R. Rajaram, J. Mathiyarasu, *Colloids Surf. B Biointerfaces*, 170 (2018) 109.
48. J. Zhao, P. Du, X. Sun, H. Liu, *Int J Electrochem Sci*, 12 (2017) 8642.